International Journal of Thermophysics, Vol. 23, No. 1, January 2002 (© 2002)

Crossover Behavior of Linear and Star Polymers in Good Solvents[1]

L. Lue[2–4] and S. B. Kiselev[3]

Monte Carlo simulation calculations for the mean-square end-to-end distance and second virial coefficient for model linear and star polymers composed of hard spheres with square-well attractions are presented. For these polymers, two types of crossover behavior are observed: (i) crossover from the Gaussian chain to the Kuhnian chain limits and (ii) crossover from the semiflexible chain to the Kuhnian chain limits. A crossover theory for the properties of dilute linear and star polymers under good solvent conditions is presented. This model directly relates the properties of the monomer–monomer interaction to the renormalized parameters of the theory. The predictions of the crossover theory are in good agreement with simulation data. A new equation of state for linear and star polymers in good solvents is presented. The equation of state captures the scaling behavior of polymer solutions in the dilute/semidilute regimes and also performs well in the concentrated regimes, where the details of the monomer–monomer interactions become important. This theory is compared to Monte Carlo simulation data for the volumetric behavior of tangent hard-sphere polymers.

KEY WORDS: computer simulation; crossover; linear polymers; penetration function; scaling; star polymers.

[1] Paper presented at the Fourteenth Symposium on Thermophysical Properties, June 25–30, 2000, Boulder, Colorado, U.S.A.

[2] Physical and Chemical Properties Division, National Institute of Standards and Technology, 325 Broadway, Boulder, Colorado 80305-3328, U.S.A.

[3] Chemical Engineering and Petroleum Refining Department, Colorado School of Mines, Golden, Colorado 80401-1887, U.S.A.

[4] To whom correpondence should be addressed at Department of Chemical Engineering, UMIST, P.O. Box 88, Manchester M60 1QD, United Kingdom. E-mail: Leo.Lue@umist.ac.uk

0195-928X/02/0100-0117/0 © 2002 Plenum Publishing Corporation

1. INTRODUCTION

For sufficiently high molecular weights, the properties of dilute polymer solutions, under good solvent conditions, exhibit universal scaling behavior [1]. For example, the mean square end-to-end distance $\langle R^2 \rangle$ has the form

$$\langle R^2 \rangle = AN^{2\nu} \tag{1}$$

where N is the degree of polymerization, ν is a univeral scaling exponent, and A is a coefficient that depends on the details of the polymer. In the absence of excluded-volume interactions, $\nu = 0.5$, and the polymer exhibits Gaussian statistics. When excluded-volume interactions are present, $\nu = 0.588$, and the polymer exhibits Kuhnian statistics [1]. Another property that exhibits scaling behavior is the pressure p of a polymer system, which is given by [1]

$$\frac{p}{k_B T c_p} = Z(c_p N^{d\nu}) \tag{2}$$

where k_B is the Boltzmann constant, T is the absolute temperature of the system, c_p is the concentration of polymer in solution, and d is the dimensionality of space. We develop a crossover theory for dilute linear and star polymer solutions, similar in form to crossover theories for critical phenomena in simple fluids. We then compare our results with Monte Carlo simulations for a simple model polymer to test the accuracy of our theory. In addition, we are able to ascertain a precise relation between the renormalized parameters of our theory and the microscopic parameters of our model polymer. The remainder of the paper is organized as follows. First, in Section 2, we provide a brief review of polymer field theory and develop a crossover theory for dilute polymer solutions. In Section 3, we present the theory for the thermodynamics of dilute to concentrated polymer solutions.

2. DILUTE POLYMER SYSTEMS

The Edwards Hamiltonian provides a coarse-grained description of a fully flexible polymer chain with excluded-volume interactions [2]. For star polymers, this generalizes to [3]

$$H[R] = \frac{1}{2} \sum_{\alpha=1}^{f} \int_0^{s_B} dt_\alpha \left(\frac{\partial R(t_\alpha)}{\partial t_\alpha} \right)^2 + \frac{v_B}{2} \sum_{\alpha,\gamma=1}^{f} \int_0^{s_B} dt_\alpha \int_0^{s_B} dt'_\gamma \delta(R(t_\alpha) - R(t'_\gamma)) \tag{3}$$

where d is the dimensionality of space, f is the number of arms on the star polymer, S_B is proportional to the molecular weight of each arm of the star polymer, v_B is an effective segment–segment interaction parameter that measures the strength of the excluded-volume interaction, and $R(t_\alpha)$ is the position of "segment" t_α on arm α of the star polymer. The first term enforces the connectivity of the polymer, and the second term accounts for excluded-volume interactions between "segments" of the polymer. Due to the coarse-grained nature of the Edwards Hamiltonian, it is limited to polymers with many statistical segments [1, 2]. Above the theta temperature, the two-body interaction constant $v_B > 0$. In this case, the model is not exactly solvable, and renormalized perturbation methods need to be used (see Ref. 1 for details).

In this method, a general property Q is given by

$$Z_Q^{-1}(u)\, Q(u, S; L) = \lim_{a \to 0} Q_B(v_B, S_B; a) \tag{4}$$

where a is a cutoff length for the model and L is the length scale at which the property is measured. The function $Z_Q(u)$ and renormalized parameters $u = v_B L^\epsilon$, where $\epsilon = 4 - d$, and $S = Nl^2/d$ of the Edwards Hamiltonian, are chosen to absorb the divergences of the model as $a \to 0$. Note that the values of the renormalized parameters u and S depend on L, but despite this, the measurable properties of the system Q should be independent of the length scale at which they are measured. This independence leads to the renormalization-group equation, which relates the model parameters u and S at length scale L to the parameters at length scale L_R (u_R and S_R), through the following equations [4]:

$$1 - Y = \bar{u}(1 - \bar{u})^{-\epsilon/2} \left(\frac{L_R^2}{L^2} \right)^{\epsilon/2} Y^{\epsilon/\omega} \tag{5}$$

$$\frac{S_R}{S} = (1 - \bar{u})^{(2-1/\nu)/\omega}\, Y^{-(2-1/\nu)/\omega} \exp[-\kappa(1 - \bar{u}) + \kappa Y] \tag{6}$$

where $\kappa = 11u^*/16$, $\bar{u} = u/u^*$, $\bar{u}_R = u_R/u^*$, and $Y = 1 - \bar{u}_R$ is the crossover function.

The best estimates of the exponents are $\nu = 0.5880$ and $\omega = 0.790$ [5]. The best estimate of the fixed point u^* is $u^* = 0.1771$ [5]. An explicit form of the crossover function depends on the match-point condition accepted in the theory. Here we choose $L_R^2 = fS_R$, and the crossover function is written in the form

$$(1 - Y)^{2/\epsilon} = \bar{N} Y^{1/\Delta} e^{\kappa Y} \tag{7}$$

where $\Delta = \omega\nu$, $\bar{N} = fN/N^*$, and N^* is given by

$$N^* = (\bar{u}\Lambda)^{-2} |1-\bar{u}|^{1/\Delta} e^{\kappa(1-\bar{u})} \tag{8}$$

where $\Lambda^{-2} = L^2 d/l^2$ is a system-dependent parameter. The crossover function Y has the following asymptotic limits:

$$Y \to \begin{cases} 1 - e^{\kappa/2}\bar{N}^{1/2} + \cdots & \text{for} \quad \bar{N} \ll 1 \\ \bar{N}^{-\Delta}[1 - \Delta(2+\kappa)\,\bar{N}^{-\Delta} + \cdots] & \text{for} \quad \bar{N} \gg 1 \end{cases} \tag{9}$$

When $Y \approx 1$, the excluded-volume interactions play a minor role, and the polymer is nearly Gaussian. When $Y \ll 1$, the excluded-volume interactions play a major role, and the polymer exhibits Kuhnian statistics. From Eq. (9), the polymer exhibits Gaussian statistics when $N^* \gg N \gg 1$. When $N \sim 1$, the chain is too short for the Edwards Hamiltonian to apply, and the statistics of the chain are no longer universal but, instead, depend strongly on the details of the chain. When the polymer exceeds a critical length, $N \gg N^*$, it exhibits Kuhnian statistics. This is in direct analogy to systems near a second-order phase transition [6].

For these systems, mean-field critical behavior is observed when $Gi \ll \tau \ll 1$, where $\tau = |T/T_c - 1|$, T is the temperature of the system, T_c is the critical temperature of the system, and Gi is the Ginzburg number. Universal critical behavior is observed when $\tau \ll Gi$. Therefore, in dilute polymer solutions, $1/N$ plays the role of τ, and $1/N^*$ is analogous to the Ginzburg number Gi. The connection between the excluded-volume interaction and the Ginzburg number has been discussed previously by other authors [7]. The usefulness of the crossover function Y lies in the fact that the properties of the polymer can be written as a universal function of Y, independently of the details of the polymer. These details are contained in the parameters $\bar{u}$ and N^*. For example, the mean-square end-to-end distance $\langle R^2 \rangle$ can be written in terms of the crossover function as [8]

$$\frac{\langle R^2 \rangle}{Nl^2} = aY_R \tag{10}$$

where the crossover function is

$$Y_R = [1 + e_1(1-Y) + e_2(1-Y)^2]\, Y^{-(2\nu-1)/\Delta} e^{\kappa Y} \tag{11}$$

the universal constants $e_1 = -0.125$ and $e_2 = 0.283$ [4], and the amplitude a is given by

$$a = |1-\bar{u}|^{(2\nu-1)/\Delta} e^{-\kappa(1-\bar{u})} \tag{12}$$

We compare our theoretical predictions against simulations for model polymers composed of rigidly bonded hard spheres. We model the star polymers as being composed of rigidly bonded hard spheres of diameter σ. The f arms of the star polymer are all attached to a central "core" sphere. Each arm consists of N spheres, and the bond length between each of the spheres is l. A schematic drawing of a model star polymer is given in Fig. 1. In Fig. 2, we plot the variation of the mean-square end-to-end and mean-square center-to-end distances for polymers of various values of σ/l as a function of the number of spheres on the polymer N. The long-dashed line represents the scaling relation given in Eq. (1) with $A = 0.792$. The simulation data for $\sigma/l > 0.447$ lie above this curve, while the data for $\sigma/l < 0.447$ lie below. The simulation data for $\sigma/l = 0.447$ lie directly on this curve.

If one were to fit an equation of the form

$$\frac{\langle R^2 \rangle}{l^2} = A_{\text{eff}} N^{2\nu_{\text{eff}}} \tag{13}$$

to the data for $\sigma/l > 0.447$, one would find an effective exponent ν_{eff} higher than the theoretical value, $\nu = 0.5880$, for finite chain lengths. As data for longer and longer length chains are fitted, the effective exponent will gradually decrease to the theoretical value ν. For systems with $\sigma/l < 0.447$, the effective exponent is lower than the actual exponent and monotonically increases to ν with increasing chain length. When $\bar{N} \gg 1$, $\langle R^2 \rangle$ can be written in Wegner scaling form:

$$\frac{\langle R^2 \rangle}{l^2} = A_0 N^{2\nu} [1 + A_1 N^{-\Delta} + \cdots] \tag{14}$$

If one fits a Wegner-type equation to the data, theoretically, one expects [4] to find a negative Wegner coefficient A_1 if $\bar{u} > 1$ and a positive Wegner coefficient if $\bar{u} < 1$. When $\bar{u} = 1$, the Wegner correction vanishes, and there is pure scaling behavior. When $\bar{N} \ll 1$, the crossover function $Y_R \approx 1$, and Eq. (10) reproduces the Gaussian limiting behavior.

$$\frac{\langle R^2 \rangle}{l^2} = aN \tag{15}$$

Therefore, the relationship between the dimensionless excluded-volume parameter $\bar{u}$ and the ratio σ/l can be found from the condition that $\bar{u}$ is, in this case, proportional to the Fixman parameter (i.e., $\bar{u} \propto z \propto (\sigma/l)^3$).

In our previous work [4], we found empirically that the hard-sphere chain most rapidly approaches the infinite molecular weight limit when $\sigma/l = 0.447$. According to the crossover theory, this corresponds to $u = u^*$.

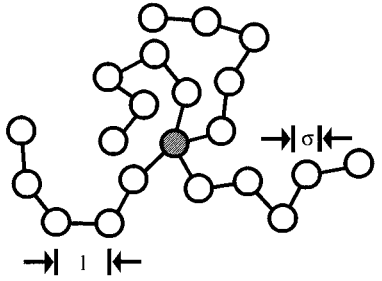

Fig. 1. Schematic drawing of a four-arm ($f = 4$) star polymer with $N = 5$ spheres per arm. The diameter of the spheres is σ, and the bond length is l. The shaded sphere is the central "core" sphere.

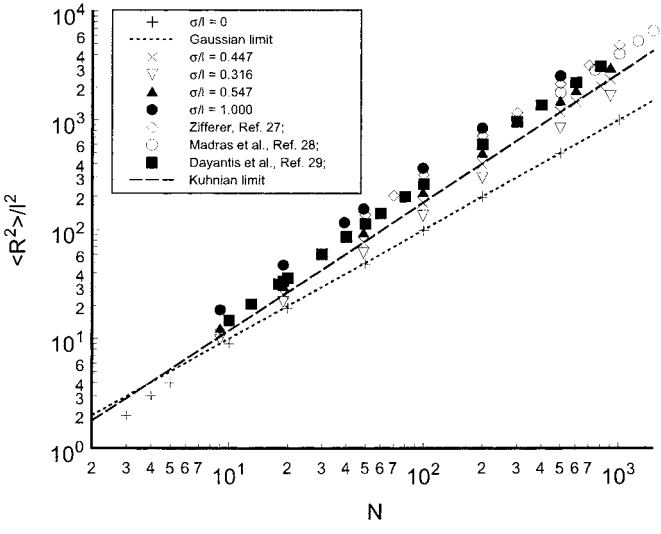

Fig. 2. Mean-square end-to-end distance, $\langle R^2 \rangle$, for various hard-sphere chains: (i) $\sigma/l = 1$ (filled circles), (ii) $\sigma/l = 0.548$ (filled triangles), (iii) $\sigma/l = 0.447$ (crosses), (iv) $\sigma/l = 0.316$ (open triangles), and (v) $\sigma/l = 0$ (pluses), (vi) tetrahedral lattice chains [27] (diamonds), (vii) sc lattice chains [28] (open circles), (viii) sc lattice chains [29] (squares), (ix) Gaussian limit (short-dashed line), and (x) Kuhninan limit (long-dashed line).

Therefore, the case $\sigma/l = 0.447$ corresponds to $\bar{u} = 1$, $\sigma/l < 0.447$ corresponds to $\bar{u} < 1$, and $\sigma/l > 0.447$ corresponds to $\bar{u} > 1$. Combining these results with the fact that $\bar{u} \propto (\sigma/l)^3$, we arrived at the relation [4]

$$\bar{u} = 11.18 \left(\frac{\sigma}{l}\right)^3 \tag{16}$$

For polymers composed of hard spheres with square-well attractions, the expression for $\bar{u}$ is slightly more complicated [9], involving also the depth and width of the attractive well. The crossover function given in Eq. (7) is based on an expansion that is valid for small values of the parameter $\bar{u}$. It is accurate only in the case $\bar{u} < 1$. The case $\bar{u} > 1$ describes the crossover behavior of a semiflexible polymer with excluded-volume interactions. The Edwards Hamiltonian, which describes fully flexible polymers, is no longer relevant, and a different Hamiltonian needs to be employed (for example, see Ref. 10). We do not consider this situation. For $\bar{u} < 1$, the crossover theory predicts that all polymer data for $\langle R^2 \rangle$ can be collapsed to a single universal function, if rescaled properly. To demonstrate this, we plot the variation of $\langle R^2 \rangle / (Na)$ with $\bar{N}$ for polymers with $\bar{u} < 1$ in Fig. 3. The symbols are the results of Monte Carlo simulations, and the line is the theoretical crossover function. The data collapse

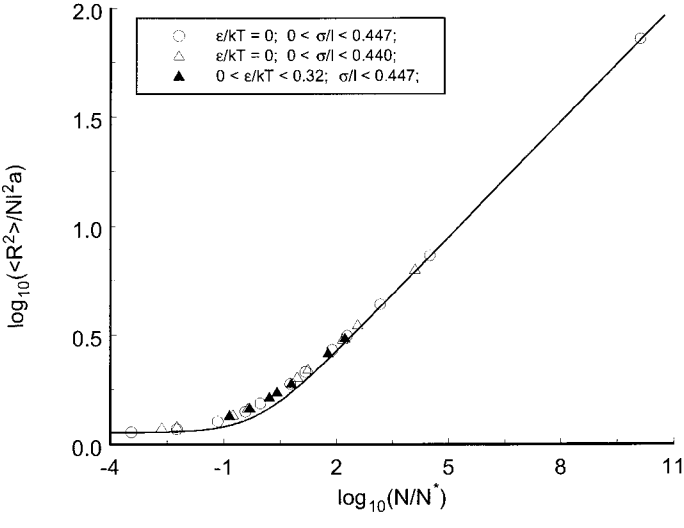

Fig. 3. Variation of the scaled mean-square end-to-end and center-to-end distances with $\bar{N}$ for polymers with $\bar{u} < 1$: (i) Monte Carlo simulation data (symbols); (ii) crossover theory with $e_1 = -0.125$ and $e_2 = 0.283$ (solid line).

onto a single universal curve, that is well described by the theory. We see the crossover from Gaussian behavior with $\langle R^2 \rangle \propto N$ when $\bar{N} \ll 1$ to Kuhnian behavior with $\langle R^2 \rangle \propto N^{2\nu}$ when $\bar{N} \gg 1$. Another quantity of interest is the penetration function Ψ, defined by [1]

$$\Psi = \left(\frac{d}{12\pi} \right)^{d/2} \frac{2B_2}{\langle R_g^2 \rangle^{d/2}} \tag{17}$$

where B_2 is the second virial coefficient between two polymers, and $\langle R_g^2 \rangle$ is the mean-square radius of gyration of the polymer.

For polymer solutions, the penetration function Ψ characterizes the solvent quality and controls the crossover behavior of the osmotic pressure in the dilute and semidilute regimes [1, 11]. The crossover expression for the penetration function of a star polymer with f arms is given by [3, 9, 12, 13]

$$\Psi = \frac{g^{d/2}}{8} (1-Y) \left[\frac{a_0 + a_1(1-Y) + a_2(1-Y)^2}{1 + b_1(1-Y) + b_2(1-Y)^2} \right] \tag{18}$$

where

$$g = \frac{f^2}{3f-2}$$

$$a_0 = 53/32$$

$$a_1 = \frac{1}{2} \ln 2 + \frac{7}{48} + \frac{13}{8} \frac{(f-1)(f-2)}{3f-2}$$

$$b_1 = \frac{1}{4} \frac{(f-1)(15f-22)}{3f-2} \ln 2 + \left(\frac{9}{8} \ln 3 - \frac{7}{4} \ln 2 \right) (f-1)(f-2) - \frac{1}{2} \ln f$$

$$a_2 = -0.087 + 2.643(f-1)(f-2)$$

$$b_2 = (0.946 + 0.213 g^{d/2})(f-1)(f-2)$$

The form for the coefficients a_2 and b_2 was not obtained theoretically; it was chosen in analogy with corresponding expressions for the coefficients a_1 and b_1, with the requirement that the resulting expression for $\Psi^*(f)$ increases monotonically with f to a finite value. Thus, our crossover model is actually a phenomenologically "repaired" crossover function, exact to second-order in ϵ.

Under good solvent conditions, the penetration function for a star polymer monotonically approaches a finite, asymptotic limiting value $\Psi^*(f)$ as its molecular weight becomes infinitely large. This limiting value

$\Psi^*(f)$ depends only on the number of arms in the star polymer and is independent of the molecular details of the polymer (as long as it is in good solvent conditions). A summary of $\Psi^*(f)$ as obtained from experimental, computer simulation, and theoretical work is given in Table I of Ref. 14. In Fig. 4, we plot the variation Ψ with the number of spheres per arm N for three-arm ($f = 3$) star polymers with various values of σ/l. For polymers with $\sigma/l < 0.447$, Ψ gradually increases with molecular weight; for $\sigma/l > 0.447$, Ψ gradually decreases with molecular weight. Regardless of the value of σ/l, however, the penetration function approaches the same asymptotic limit as the molecular weight becomes infinitely large. The closer the value of σ/l is to 0.447, the more rapidly the penetration function approaches its asymptotic value. Precisely at this critical value of σ/l, $\Psi(f = 3)$ remains roughly constant, nearly equal to its asymptotic value $\Psi^*(f = 3)$ for almost all molecular weights.

This same qualitative behavior is observed for linear polymers [4, 9, 15] and star polymers of differing number of arms. The value of σ/l that corresponds to $\bar{u} = 1$ (i.e., $\sigma/l = 0.447$) is independent of the number of arms f on the star polymer; however, the asymptotic limiting value $\Psi^*(f)$ of the penetration function is dependent on f. Therefore, we find that $\bar{u} = 1$ when $\sigma/l = 0.447$, independent of the number of arms on the star polymer.

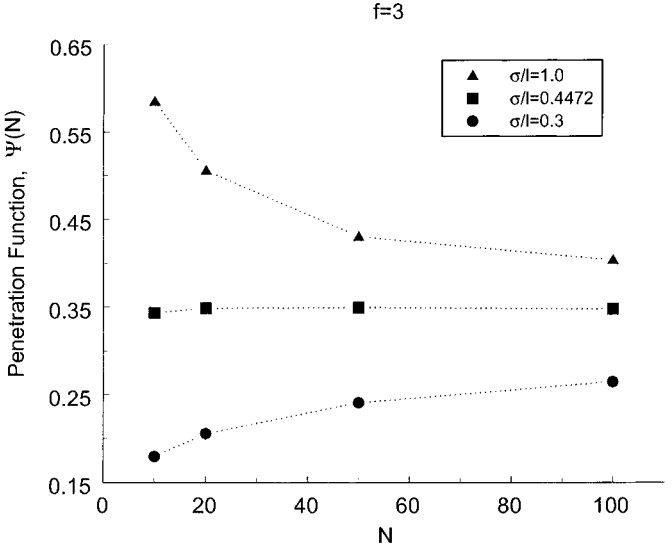

Fig. 4. Variation of the penetration function with the degree of polymerization N for three-arm stars: (i) $\sigma/l = 0.3$ (circles), (ii) $\sigma/l = 0.447$ (squares), and (iii) $\sigma/l = 1.0$ (triangles).

Table I. Monte Carlo Simulation Estimate of Ψ^*

f	Ψ^*
1, 2	0.25 ± 0.01
3	0.359 ± 0.004
4	0.453 ± 0.007
5	0.553 ± 0.006
6	0.63 ± 0.01
12	1.057 ± 0.008
14	1.160 ± 0.009
16	1.259 ± 0.009
18	1.33 ± 0.01

This is consistent with the value found from $\langle R^2 \rangle$. Our Monte Carlo simulation data for $\Psi^*(f)$ for star polymers are summarized in Table I and are shown in Fig. 5. For $f \leqslant 6$ these values are in good agreement with the simulation data of Ref. 14, however, for $f \geqslant 12$ our data lie systematically above the simulation data of Ref. 14. We think that the data in Ref. 14 at $f = 12$ and 18 most likely correspond to finite-size stars under conditions where $\bar{u} < 1$, for which Ψ has not yet approached Ψ^*.

As a comparison, we also show in Fig. 5 the predictions obtained by Douglas and Freed [13], given by the dashed–dotted line. The predictions of Douglas and Freed are systematically higher than the simulation data, and the difference between them increases dramatically for $f \geqslant 6$. In the limit $f \to \infty$, Eq. (18) with the parameters found from a fit to the data of Ref. 14 yields $\Psi^*(f \to \infty) = 1.55$, which is close to the hard-sphere limit $\Psi_{\text{HS}} = 1.619$ [16]. Roovers and co-workers suggest [17] that $\Psi^*(f \to \infty)$ should be precisely equal to the penetration function for hard spheres; however, others have pointed out that there is no justification that these two values should be exactly the same [13]. Using Daoud–Cotton theory [18], Ohno and co-workers [16] estimate $\Psi^*(f \to \infty) = 2.13$, which is closed to the value $\Psi^*(\infty) = 2.1$ obtained with Eq. (18) with the parameters found from a fit to our data. For a more accurate determination of $\Psi^*(\infty)$ we need more data for $f \geqslant 18$.

Figure 6 compares simulation data for $0.1 \leqslant \sigma/l < 0.447$ to the rescaled values of the penetration function, $\bar{\Psi} = \Psi(\bar{N}, f)/\Psi^*(f)$, calculated with Eq. (18). The predicted values of the penetration function are in fairly good agreement with the simulation data; however, there are systematic deviations. These systematic deviations can be eliminated if the experimental values of the parameter $\bar{N}$ are rescaled by a factor of 3.5 (i.e., $\bar{N}_{\text{exp}} = 3.5(fN/N^*)$). This corresponds to choosing a match point of $L_R^2 = 3.5 f S_R$

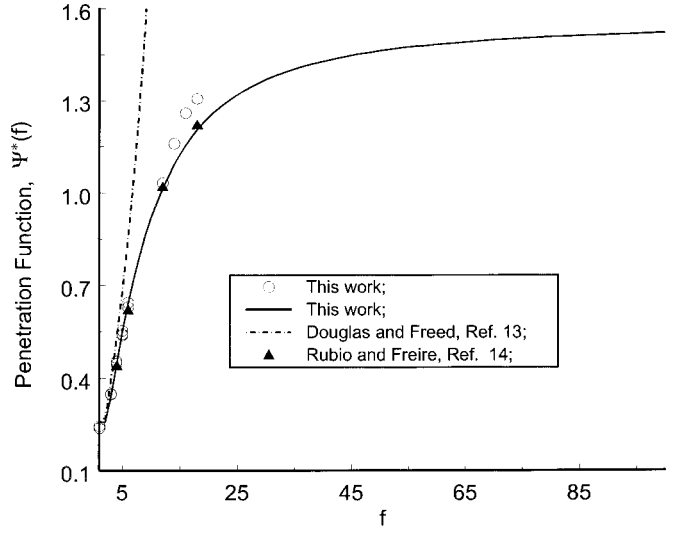

Fig. 5. Variation of the infinite molecular weight limit of the penetration function $\Psi^*(f)$ for star polymers with f arms: (i) simulation data (symbols), (ii) calculated values from Eq. (18) (solid line), and (iii) calculated values of Douglas and Freed (dashed line).

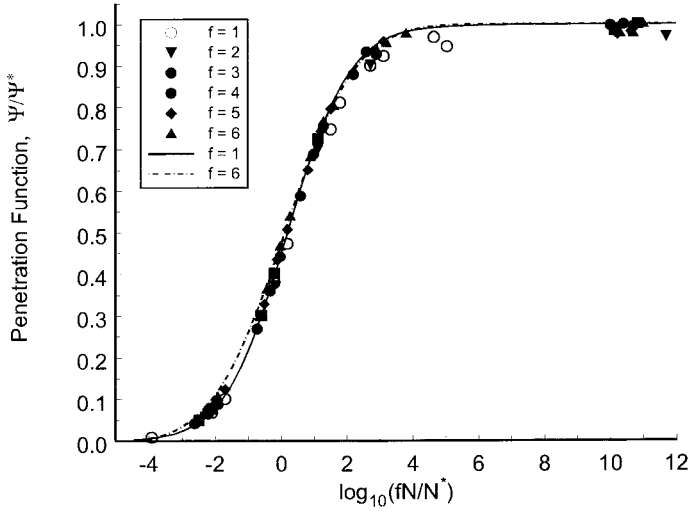

Fig. 6. Variation of the rescaled penetration function $\bar{\Psi}(\bar{N}, f) = \Psi(\bar{N}, f)/\Psi^*(f)$ with the rescaled degree of polymerization $\bar{N} = fN/N^*$: (i) simulation data (open symbols), (ii) rescaled simulation data (filled symbols), and (iii) calculated values (lines).

in Eq. (5), rather than $L_R^2 = fS_R$. After this rescaling, excellent agreement between the simulation data (filled symbols in Fig. 6) and the calculated values of the penetration function is obtained over the entire range of $\bar{N}$.

3. POLYMER SOLUTIONS

In the dilute and semidilute regimes, the connectivity of the polymers induce long-range correlations between the monomer segments. The details of the monomer–monomer interactions do not play a major role; thus, a coarse-grained description of the polymers, such as the Edwards Hamiltonian [2, 3], can be used. It can be shown [19, 20] that, to one-loop order, the Helmholtz free energy F of a linear or star polymer solution, in the dilute to semidilute regimes, is given by

$$\frac{F}{k_B TV} = c_p \left[\ln \frac{c_p}{Q} - 1 \right] + c_p X \exp\left[-\frac{\kappa \bar{\Psi}}{4} A(X) \right] \tag{19}$$

where V is the volume of the system, Q is the partition function of an isolated, self-interacting chain, c_p is the number density of polymer molecules in the system, $X = B_2 c_p$, $\bar{\Psi} = \Psi(N, f)/\Psi^*(f)$ is a scaled penetration function, $\kappa = (2-dv)/(dv-1) \approx 0.3089$ is a universal constant, and $A(x) = x^{-2}[2x + 6x^2 - (1+2x)^2 \ln(1+2x)]$. The corresponding expression for the compressibility factor Z is

$$Z = 1 + X \left[1 + \frac{\kappa \bar{\Psi}}{2} B(X) \right] \exp\left[-\frac{\kappa \bar{\Psi}}{4} A(X) \right] \tag{20}$$

where $B(x) = x^{-2}[2x + 2x^2 - (1+2x)\ln(1+2x)]$. This free-energy model was developed by combining "infinite" order expressions with first order calculations [19], and as a result, it agrees with the theoretical scaling results [1, 5].

In this theory, the polymer architecture does not enter explicitly into the thermodynamic properties of the system. The only distinction between different architectures is the asymptotic limit of the penetration function Ψ^*. All polymers, regardless of architecture, should approach the same limiting form of the equation of state in the dilute/semidilute regimes as the molecular weight of the polymer becomes infinitely high. Recall that for stiff polymers, $\bar{\Psi} > 1$, and it decreases gradually to $\bar{\Psi} = 1$ as the molecular weight increases. For fully flexible polymers, $\bar{\Psi} < 1$, and it increases gradually as the molecular weight increases. Therefore, for stiff

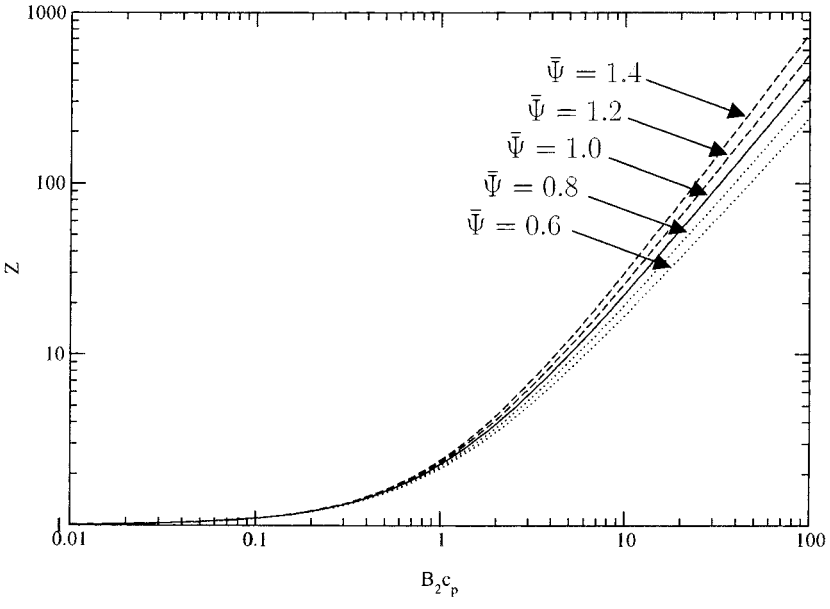

Fig. 7. Deviation of the equation of state from the infinite molecular weight limit: (i) $\bar{\Psi} = 1$, infinite molecular weight limit (solid line), (ii) $\bar{\Psi} > 1$, stiff polymer of finite molecular weight (dashed lines), and (iii) $\bar{\Psi} < 1$, flexible polymer of finite molecular weight (dotted lines).

polymers in the dilute/semidilute regime, we expect the compressibility factor to decrease to the infinite molecular weight limit as the molecular weight of the polymer increases, while for flexible polymers, we expect the compressibility factor to increase. This is shown in Fig. 7, where the dashed lines represent polymer systems with $\bar{\Psi} > 1$, the dotted lines represent systems with $\bar{\Psi} < 1$, and the solid line is a system with $\bar{\Psi} = 1$ (infinite molecular weight limit). In the concentrated regime, where the details of the monomer–monomer interactions become important, the expression for the Helmholtz free energy given in Eq. (19) breaks down.

In Ref. 19, we demonstrated how the renormalization procedure used in the polymer field theory could be applied to a liquid-state theory approach, which includes details of the monomer–monomer interactions. This led to the following expression for the residual Helmholtz free energy F^{res}:

$$\beta F^{\text{res}}(T, c_p) = \beta F^{\text{res}}_{\text{ref}}(T, Nc_p) + \frac{V}{2} N^2 \hat{f}(0)\, c_p^2 + V c_p \bar{X} \exp\left[-\frac{\kappa \bar{\Psi}}{4} A(\bar{X}) \right] \tag{21}$$

where $F_{\text{ref}}^{\text{res}}$ is the residual Helmholtz free energy of a disconnected monomer fluid, $\bar{X} = B_2 c_p \Gamma_1$, $\Gamma_1 = \hat{h}_{\text{ref}}(0)/\hat{f}(0)$, $\hat{f}(0)$ is the zero-wave vector value of the Mayer f-function of the monomer–monomer interaction, and $\hat{h}_{\text{ref}}(0)$ is the zero-wave vector value of the total correlation function of a disconnected monomer fluid. The equation of state is given by

$$Z = 1 + NZ_{\text{ref}}^{\text{res}}(T, Nc_p) + \frac{1}{2}\hat{f}(0)\, N^2 c_p + \bar{X}(1+\Gamma_2)\left[1 + \frac{\kappa\bar{\Psi}}{4} B(\bar{X})\right] \exp\left[-\frac{\kappa\bar{\Psi}}{4} A(\bar{X})\right] \tag{22}$$

where $Z_{\text{ref}}^{\text{res}}$ is the residual compressibility factor for the disconnected monomer fluid, and $\Gamma_2 = \partial \ln \Gamma_1 / \partial \ln(Nc_p)$. Note that this expression inherently assumes that $\hat{f}(0) < 0$, which corresponds to polymers in good solvent conditions. In addition, this expression assumes that the polymer molecular weight is high. This expression is valid for polymer solutions in the dilute to concentrated regimes.

We compare our theory with simulation data for tangent hard-sphere chains. For this system, the reference fluid is the hard-sphere fluid, which is well described by the Carnahan–Starling equation of state [21],

$$Z_{\text{HS}}^{\text{res}} = \frac{2y(2-y)}{(1-y)^3} \tag{23}$$

where $y = \pi\sigma^3 c_p/6$ is the fraction of space occupied by the spheres. For this equation of state, the functions Γ_1 and Γ_2 are given by

$$\Gamma_1 = \frac{1 - y/4}{1 + 4y + 4y^2 - 4y^3 + y^4} \tag{24}$$

and

$$\Gamma_2 = -\frac{y(17 + 32y - 52y^2 + 24y^3 - 3y^4)}{(4-y)(1 + 4y + 4y^2 - 4y^3 + y^4)} \tag{25}$$

In Fig. 8, we plot the equation of state of fluids composed of tangent hard-sphere chains with $N = 51$ and $N = 201$ in the concentrated regime. The symbols are the results from computer simulations by various researchers. The solid lines are the predictions of Eq. (22), and the dashed lines are the predictions of the commonly used thermodynamic perturbation theory (TPT) equation of state for tangent hard-sphere chains [22]. The values for the second virial coefficient and penetration function used in Eq. (22) were taken from Refs. 19 and 23.

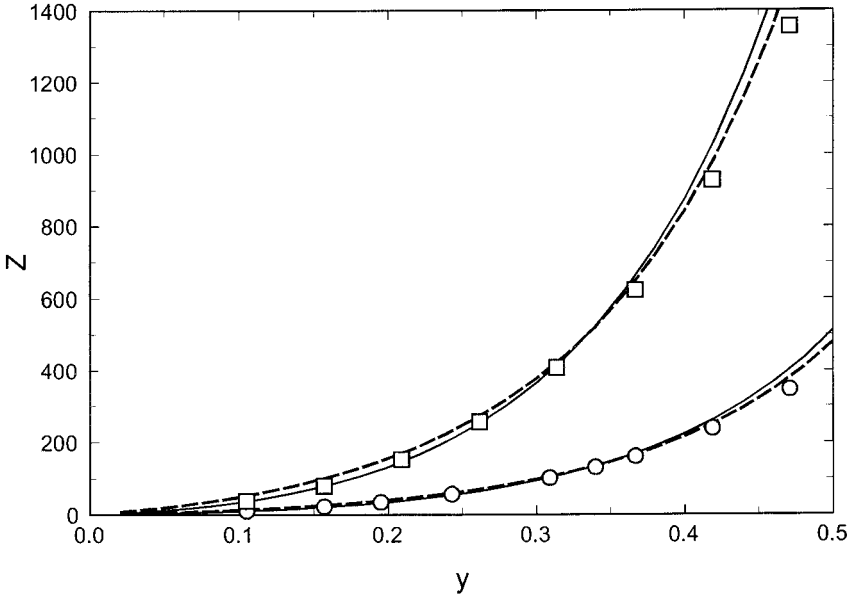

Fig. 8. Equation of state for tangent hard-sphere chains of various degrees of polymerization. The symbols are the results of computer simulations for (i) $N = 51$, Ref. 30 (circles), and (ii) $N = 201$, Ref. 30 (squares). The solid lines are the predictions of Eq. (22), and the dashed lines are the predictions of the TPT equation of state.

For packing fractions $y \leqslant 0.3$, the predictions of Eq. (22) are in slightly better agreement than the TPT equation of state with the simulation data. Even for chains as short as $N = 4$, the crossover equation of state still yields reasonable results [19]. At higher packing fractions, the predictions of Eq. (22) become slightly worse than the TPT equation of state, although they both overpredict the pressure of the system. In Fig. 9, we plot the equation of state of tangent hard-sphere chains of different lengths, from the dilute to concentrated regimes. The symbols are the results of the Monte Carlo simulations, and the lines are the predictions of Eq. (22). As the molecular weight of the chain becomes infinite, the compressibility factor approaches a universal function of $B_2 c_p$, given by the dashed–dotted line. The open symbols, which represent systems in the dilute/semidilute regimes, where $y \ll 1$, lie approximately on a single, universal curve. This behavior is also observed experimentally for polymers in good solvents [1]. As the fraction of space occupied by the monomers increases, the equation of state deviates from the universal curve: as N decreases, the deviation occurs at a lower value of X. As can be seen, the predictions of Eq. (22) agree well with the simulation data.

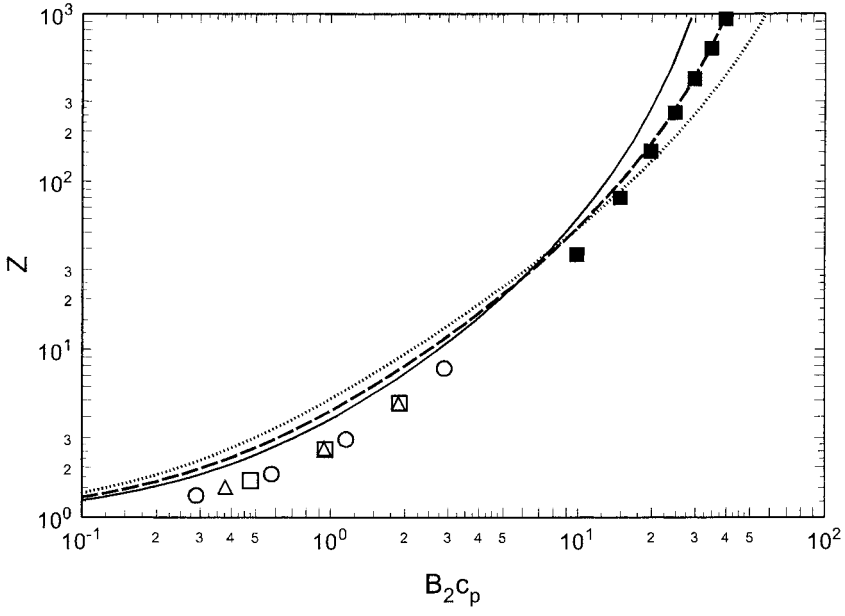

Fig. 9. Equation of state of tangent hard-sphere chains in the dilute to concentrated regimes. The symbols are the results of computer simulations for $N = 100$ (circles), $N = 200$ (squares), and $N = 500$ (triangles). The open symbols represent systems in the dilute/semidilute regimes, and the filled symbols represent systems in the concentrated regime. The lines are the predictions of Eq. (22) for $N = 100$ (solid line), $N = 200$ (dashed line), $N = 500$ (dotted line), and $N \to \infty$ (dashed–dotted line).

In Fig. 10, we compare the predictions of the TPT equation of state for dilute/semidilute tangent hard-sphere systems with Monte Carlo simulation data. In the dilute and semidilute regions, the TPT equation of state overpredicts the pressure of the system, and the results steadily worsen with decreasing polymer concentration and with increasing N. This can be traced to the fact that the TPT equation possesses a second virial coefficient B_2 which scales incorrectly with the degree of polymerization ($B_2 \propto N^2$ rather than $B_2 \propto N^{dv}$) and, therefore, overpredicts the second virial coefficient for large molecular weights. As a result, the TPT equation of state does not yield the correct universal form for dilute to semidilute solutions of high molecular weight polymers [see Eq. (20)]. This conclusion applies to all equations of state that possess a second virial coefficient that scales with molecular weight as $B_2 \propto N^2$. Thus, these types of equations of state cannot properly describe the behavior of dilute to semidilute polymer systems.

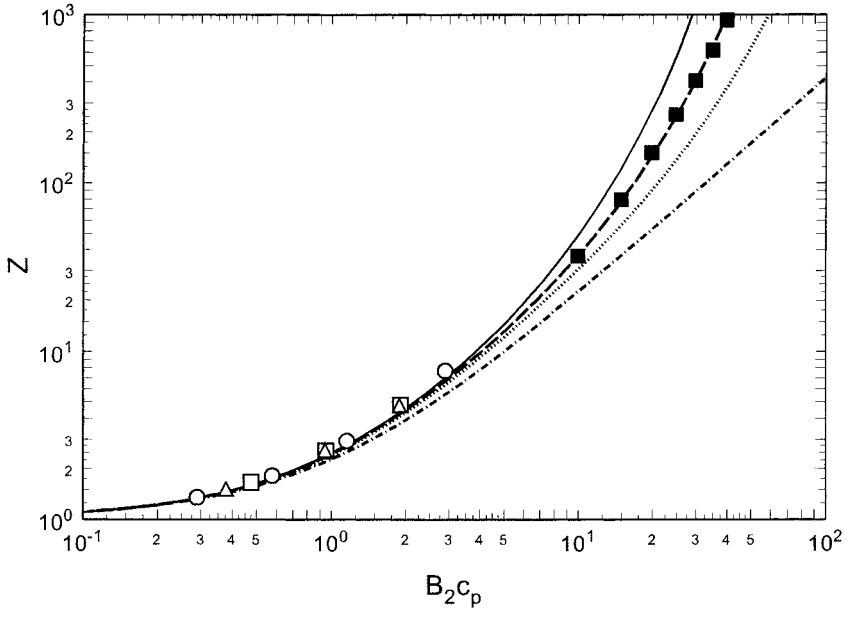

Fig. 10. Equation of state of tangent hard-sphere chains in the dilute to concentrated regimes. The symbols are the results of computer simulations for $N = 100$ (circles), $N = 200$ (squares), and $N = 500$ (triangles). The open symbols represent systems in the dilute/semi-dilute regimes, and the filled symbols represent systems in the concentrated regime. The lines are the predictions of the TPT equation of state for $N = 100$ (solid line), $N = 200$ (dashed line), and $N = 500$ (dotted line).

ACKNOWLEDGMENT

The research at the Colorado School of Mines was supported by the Office of Basic Energy Sciences of the U.S. Department of Energy under Grant DE-FG03-95ER14568.

REFERENCES

1. P.-G. de Gennes, *Scaling Concepts in Polymer Physics* (Cornell, Ithaca, New York, 1979); K. F. Freed, *Renormalization Group Theory of Macromolecules* (John Wiley and Sons, New York, 1987); J. des Cloizeaux and G. Jannink, *Polymers in Solution: Their Modeling and Structure* (Clarendon Press, Oxford, 1990).
2. S. F. Edwards, *Proc. Phys. Soc.* **85**:613 (1965); *Proc. Phys. Soc.* **88**:265 (1966).
3. A. Miyake and K. F. Freed, *Macromolecules* **16**:1228 (1983).
4. L. Lue and S. B. Kiselev, *J. Chem. Phys.* **110**:2684 (1999).
5. J. C. L. Guillou and J. Zinn-Justin, *Phys. Rev. Lett.* **39**, 95 (1977).
6. M. Y. Belyakov and S. B. Kiselev, *Physica A* **190**:75 (1992); M. A. Anisimov, S. B. Kiselev, J. V. Sengers, and S. Tang, *Physica A* **188**:487 (1992).

7. J. Dudowicz, M. Lifschitz, K. F. Freed, and J. F. Douglas, *J. Chem. Phys.* **99**:4804 (1993).
8. A. L. Kholodenko and K. F. Freed, *J. Chem. Phys.* **78**, 7390 (1983).
9. L. Lue and S. B. Kiselev, *J. Chem. Phys.* **111**:5580 (1999).
10. A. L. Kholodenko, *J. Chem. Phys.* **95**:628 (1991).
11. B. J. Cherayil, M. G. Bawendi, A. Miyake, and K. F. Freed, *Macromolecules* **19**:2770 (1986).
12. L. Lue and S. B. Kiselev, *J. Chem. Phys.* **114**:5026 (2001).
13. J. F. Douglas and K. F. Freed, *Macromolecules* **17**:1854 (1984).
14. A. M. Rubio and J. J. Freire, *Macromolecules* **29**:6946 (1996).
15. L. Schäfer, *Phys. Rev. E* **50**:3517 (1994); B. Krüger and L. Schäfer, *J. Phys. I France* **4**:757 (1994); B. Krüger and L. Schäfer, *Macromolecules* **29**:4737 (1996); P. Grassberger, P. Sutter, and L. Schäfer, *J. Phys. A Math. Gen.* **30**:7039 (1997); L. Schäfer, *Phys. Rep.* **301**:205 (1998)
16. K. Ohno, K. Shida, M. Kimura, and Y. Kawazoe, *Macromolecules* **29**:2269 (1996).
17. J. Roovers, N. Hadjichristidis, and L. J. Fetters, *Macromolecules* **17**:214 (1983).
18. M. Daoud and J. P. Cotton, *J. Phys.* **43**:531 (1982).
19. L. Lue, *J. Chem. Phys.* **112**:3442 (2000); C. S. Patrickios and L. Lue, *J. Chem. Phys.* **113**:5485 (2000).
20. T. Ohta and Y. Oono, *Phys. Lett.* **89A**:460 (1982).
21. N. F. Carnahan and K. E. Starling, *J. Chem. Phys.* **51**:635 (1969).
22. D. Ghonasgi and W. G. Chapman, *J. Chem. Phys.* **100**, 6633 (1994).; W. G. Chapman, G. Jackson, and K. E. Gubbins, *Mol. Phys.* **65**:1057 (1988).
23. J. Dautenhahn and C. K. Hall, *Macromolecules* **27**:5399 (1994).
24. L. Schäfer, *Macromolecules* **15**:652 (1982).
25. P. Wiltzius, H. R. Haller, D. S. Cannell, and D. W. Schaefer, *Phys. Rev. Lett.* **51**:1183 (1983).
26. Y. Shiwa, Y. Oono, and P. R. Baldwin, *Modern Phys. Lett. B* **4**:1421 (1990).
27. G. Zifferer, *Macromolecules* **23**:3166 (1990).
28. N. Madras and A. D. Sokal, *J. Stat. Phys.* **50**:109 (1988).
29. J. Dayantis and J.-F. Palierne, *J. Chem. Phys.* **95**:6088 (1991).
30. J. Gao and J. H. Wiener, *J. Chem. Phys.* **91**:3168 (1989).